

Metal Factories in the Early Universe

Stephen Eales,^{1*} Haley Gomez,¹ Loretta Dunne,¹ Simon Dye,² and Matthew W. L. Smith¹

¹*Cardiff Hub for Astrophysics Research and Technology, Cardiff University, The Parade, Cardiff CF24 3AA, UK*

²*School of Physics and Astronomy, University of Nottingham, University Park, Nottingham NG7 2RD, UK*

Accepted XXX. Received YYY; in original form ZZZ

ABSTRACT

We have measured the mass of metals in 13 submillimetre galaxies at $z \sim 4$ in which the gas, based on previous observations, lies in a cold rotating disk. We measured the metal masses using either the submillimetre line or continuum emission from three tracers of the overall metal content - carbon atoms, carbon monoxide molecules and dust grains - using the first calibration of this technique that treats all three tracers simultaneously (Dunne et al. 2022). We obtain very similar mass estimates from the different tracers, which are similar to the entire metal content of a present-day massive early-type galaxy. We used the dynamical masses of these galaxies to set an upper limit on the mass of the interstellar medium in each galaxy, allowing us to set a lower limit on the metal abundance of the ISM, finding values for many of the galaxies well above the solar value. The only caveat to this result is that we cannot be certain for all galaxies that the emission from the tracer comes from within the region covered by the dynamical analysis. Our high values for the metal abundance are supported by a recent JWST study of one galaxy which measured a super-solar metal abundance consistent with our limit. Using two chemical evolution models, we show that the high metal masses and metal abundances are what is expected shortly after the formation of a galaxy for a top-heavy IMF. We suggest a scenario for galaxy evolution in which massive galaxies reach a high metal abundance during their formation phase, which is then gradually reduced by dry mergers with lower mass galaxies. We use the chemical-evolution models to show that the metals in the outflows from massive early-type galaxies in their formation phase can quantitatively explain the long-standing puzzle that such a large fraction (≈ 0.75) of the metals in clusters of galaxies is in the intracluster gas rather than in the galaxies themselves.

Key words: galaxies: ISM – galaxies: high-redshift – galaxies: evolution – submillimetre: galaxies – galaxies: formation – galaxies: abundances

1 INTRODUCTION

One of the most distinctive properties of the galaxy population today is the strong relationship between metal abundance and stellar mass, with metal abundance increasing with stellar mass and reaching a value of about twice the solar value at the highest masses (Gallazzi et al. 2005). There is evidence that this relationship already existed for galaxies at $z \sim 3 - 5$, although with the metal abundances a factor of ≈ 4 lower than for galaxies with the same stellar mass in the universe today (Cullen et al. 2019). These relationships should be a good test of any theory of galaxy evolution, although in practice it is possible to explain them in a number of different ways (Maiolino & Mannucci 2019). Recent observations with the James Webb Space Telescope (JWST) have measured metal abundances in galaxies at $z \sim 7 - 8$, confirming the picture that the metal abundances of high-redshift galaxies are generally lower than for ones at the present day, although the metal abundances of galaxies at $z \sim 7 - 8$ are not clearly lower than those of galaxies at $z \sim 2 - 3$ (Arellano-Córdova et al. 2022; Curti et al. 2023; Carnall et al. 2023; Heintz et al. 2022; Schaefer et al. 2022; Tacchella et al. 2022; Taylor et al. 2022). Lower metal abundances for galaxies at high redshifts are, of course, not

really surprising because there has been less time then for metals to have been made in stars and ejected into the ISM.

Nevertheless, there are signs in the universe today that there must have been a period of rapid metal production early in the history of the universe. The best evidence comes from rich clusters of galaxies, in which the strong gravitational fields ensure that no metals should have been lost from the cluster. In nearby rich clusters, roughly 75 per cent of the metals are in the intracluster gas rather than in the galaxies (Portinari et al. 2004; Loewenstein 2013; Renzini & Andreon 2014; Mernier & Biffi 2022). Clusters today are dominated by elliptical and lenticular galaxies - early-type galaxies - in which the current rate of star formation, and therefore metal production, is low. The best estimates, based on the spectra of these galaxies, suggest that most of the stars were formed during the first two billion years after the big bang (Thomas et al. 2010). It therefore seems likely that most of the metals that are in the intracluster gas were formed during this early period of star formation and then ejected from the galaxies, although models based on this assumption have so far failed to reproduce the mass of metals in the intracluster gas by a factor of between 2 and 10 (Loewenstein 2013; Renzini & Andreon 2014).

Twenty-five years after they were discovered, the galaxies revealed by the first submillimetre surveys (Smail et al. 1997; Hughes et al. 1998; Barger et al. 1998; Eales et al. 1999) still seem likely to be the ancestors of the most massive early-type galaxies (Hughes et al.

* E-mail: steve.a.eales@gmail.com

1998; Lilly et al. 1999). The stellar populations and metal abundance ratios revealed by optical spectra of the most massive galaxies in present-day clusters imply that most of the stars in one of these galaxies must have formed during the first two billion years after the big bang during a burst of star formation of only $\approx 5 \times 10^8$ years (Thomas et al. 2010), requiring a star-formation rate of 100-1000 $M_{\odot} \text{ year}^{-1}$. The ‘submillimetre galaxies’ (henceforth SMGs) are still the only high-redshift galaxies with the necessary star-formation rates, and the wide-field submillimetre surveys with the *Herschel Space Observatory* and the South Pole Telescope have discovered many examples with a star-formation rate $> 1000 M_{\odot} \text{ year}^{-1}$ (Bakx et al. 2018; Reuter et al. 2020).

The high-redshift SMGs must contain a large mass of dust, which is mostly composed of metals, and they are therefore an exception to the metal-poor high-redshift universe revealed by the early JWST observations. The dust, however, makes it challenging to use standard optical techniques to measure the metal abundance, with estimates of the visual extinction often having extreme values (e.g. $A_V > 450$ - Harrington et al. (2021)). On top of this problem, there is the additional problem that many of the brightest SMGs are gravitationally lensed, which means there is a bright galaxy sitting in front of the SMG, contaminating its optical emission.

In this paper, we have developed an alternative way of measuring the mass of metals and the metal abundance in these galaxies. A standard technique for estimating the mass of the ISM in a galaxy is to use a tracer of the ISM, using the luminosity of the tracer to estimate the ISM mass. Carbon monoxide molecules (Bolatto et al. 2013), carbon atoms (Papadopoulos & Greve 2004), and dust grains (Eales et al. 2012) have all been used as tracers. An objection to this method when it is applied to a high-redshift galaxy is that it is almost always calibrated on observations in the Galaxy, and so it is often necessary to assume that the metal abundance in the high-redshift galaxy is the same as in the Galaxy (Scoville et al. 2016, 2017), which may not be true.

This objection can be neatly sidestepped if the method is used to estimate the mass of the metals rather than the mass of the ISM, since when the method is used in this way it does not rely on any assumption about the metal abundance. Using the first calibration of the method that calibrates all the tracers above simultaneously (Dunne et al. 2022), we have used this method to estimate the mass of metals in a sample of SMGs at $z \sim 4$. An advantage of our approach is that all the observations are in the submillimetre waveband, so are unobscured by the dust in the SMG, and there is also negligible contamination by emission from any gravitational lens.

This method, of course, is a way of estimating the total mass of metals but not the metal abundance, which does require knowledge of the mass of the ISM. However, a large proportion of the extreme SMGs discovered with *Herschel* and the South Pole Telescope are magnified by gravitational lenses, which has made it possible to investigate the motion of the gas with resolution as high as 50 parsec (Dye et al. 2015). Observations of the gas kinematics have revealed that the gas in many of these galaxies is distributed in a cold rotating disk (Hodge et al. 2012; Dye et al. 2015; Rizzo et al. 2020; Neeleman et al. 2020; Fraternali et al. 2021; Rizzo et al. 2021; Lelli et al. 2021; Dye et al. 2022), which makes it possible to estimate the mass of the galaxy from the circular velocity of the gas. We have selected a sample of SMGs for which there is good evidence that the gas lies in a rotating disk. By estimating the dynamical mass of each galaxy, we have put an upper limit on the mass of the ISM, which has allowed us to put a lower limit on the metal abundance.

The arrangement of the paper is as follows. §2 describes our sample of galaxies. In §3 we describe our method for estimating the mass

Table 1. The Sample

Source	Redshift	Gravitational Magnification	Reference
SPT0113-46	4.233	23.86 ± 0.51	1
ALESS073.1	4.76		2
SPT0345-47	4.296	7.95 ± 0.48	1
SPT0418-47	4.225	32.7 ± 2.66	1
SPT0441-46	4.48	12.73 ± 0.96	1
DLA0817g	4.26		3
SDP81	3.042	15.9 ± 0.7	4
AZTEC/C159	4.57		5,6
J1000+0234	4.54		5,6
GN20	4.05		7
ID141	4.24	5.5^a	8
SPT2132-58	4.768	5.72 ± 0.54	1
SPT2146-55	4.567	6.65 ± 0.41	1

Notes: a - Dye et al. (2022) do not give an error for the gravitational magnification factor, but all the ISM and metal masses in this paper have been calculated from demagnified fluxes which have errors that incorporate the uncertainties in the lensing model. Also note that the ISM masses given by Dye et al. (2022) do not include a correction for the effect of the cosmic microwave background (§3.2).

References: 1 - Reuter et al. (2020); 2 - Lelli et al. (2021); 3 - Neeleman et al. (2020); 4 - Dye et al. (2015); 5 - Jones et al. (2017), 6 - Fraternali et al. (2021); 7 - Hodge et al. (2012); 8 - Dye et al. (2022).

of metals and the application of this method to our sample. In §4, we use the dynamical masses of the galaxies to set an upper limit on the mass of the ISM of each galaxy and thus a lower limit on the galaxy’s metal abundance. In this section, we also propose a solution to the well known paradox that the estimate of the mass of the ISM in a high-redshift galaxy is often greater than its dynamical mass. In §5, we use chemical evolution models to interpret our results. In §6 we discuss our results and we list our conclusions in §7. We used the cosmological parameters given in Planck Collaboration et al. (2016).

2 THE SAMPLE

We selected a sample of 13 high-redshift galaxies for which there is evidence from the velocity profile (velocity versus radius) and from the high value of the ratio of rotational velocity to velocity dispersion (§4.1) that the gas in the galaxy lies in a cold rotating disk (Table 1). All the galaxies also have observations that make it possible to estimate the mass of the ISM in the galaxy, having at least one, and in most cases more than one, of the following observations: spectral line observations of C I; spectral line observations of CO; continuum observations of dust. Eight of the 13 galaxies are gravitationally lensed, and for each of these there is a lensing model with an estimate of the magnification and its uncertainty (Table 1). Twelve of the sample are at $z > 4$ when the universe was less than 1.6 billion years old.

3 METAL MASSES

3.1 The Method

Since molecular hydrogen does not itself emit spectral lines at the typical temperature of the ISM, the standard method to estimate the

Table 2. Continuum Measurements from Observations in the ALMA Archive

Source	Frequency (GHz)	Flux density (μ Jy)
ALESS 073.1	92.74	136 ± 22
J1000+0234	103.345	180 ± 31
SDP81	88.850	676 ± 98

mass of the ISM is from the luminosity (L) of some ‘tracer’. The mass of the ISM is then given by the equation:

$$M_{\text{ISM}} = \alpha L \quad (1)$$

in which α is a calibration factor. Carbon atoms (C I), CO and dust grains have all been used as tracers. The calibration factor is almost always ultimately based on observations of the ISM in the Galaxy, from which it is possible to estimate the ISM mass more directly, for example from gamma-ray observations or from the dynamical masses of molecular clouds (Bolatto et al. 2013; Tacconi et al. 2020). Over the last decade the application of this technique to high-redshift galaxies has led to the conclusion that as much as 90 per cent of the baryonic mass in a high-redshift galaxy is in the form of gas (Scoville et al. 2016, 2017; Tacconi et al. 2018).

An obvious concern with this technique, especially when it is applied at high redshift, is the effect of metal abundance. All of the tracers above are made of metals, which are made in stars, and it therefore may be dangerous to assume that for a galaxy at high redshift, when there has been much less time since the big bang to make metals, the value of α is the same as in the Milky Way. Nevertheless, although sometimes an attempt is made to correct the value of α using a measurement of the metal abundance (Tacconi et al. 2020), the value of the metal abundance is rarely known, and the standard optical techniques for estimating metal abundance all themselves have large systematic uncertainties (Maiolino & Mannucci 2019). Therefore, for the want of anything better, the assumption that the calibration factors have the same values as in the Galaxy is the one that is often made.

In this paper, we try to avoid this problem by using observations of the tracers to estimate the mass of the metals rather than the mass of the ISM. We calculate the mass of metals in a galaxy from the luminosity of a tracer, L using the equation:

$$M = \alpha_{\text{MW}} A_{\text{MW}} L \quad (2)$$

In this equation, α_{MW} is the same calibration factor as in equation (1), to which we have added a subscript to show it is ultimately based on observations in the Galaxy (Milky Way), and A_{MW} is the metal abundance in the ISM in the Galaxy. We assume a metal abundance in the ISM in the Galaxy of 86.9, based of the latest estimates of the gas-to-dust ratio (167.2) and the fraction of the metals that is incorporated in the dust (0.52) (Roman-Duval et al. 2022).

This equation should still be correct if the metal abundance in the galaxy that is being observed, A_{gal} , is different from the value in the Galaxy. For the optically-thin tracers, dust and C I (Harrington et al. 2021; Papadopoulos et al. 2022), the value of the calibration factor for the galaxy, α_{gal} , will be inversely proportional to the galaxy’s metal abundance, and therefore $\alpha_{\text{gal}} A_{\text{gal}} = \alpha_{\text{MW}} A_{\text{MW}}$. This is not so obviously true for CO because the line emission is optically thick. Nevertheless, although the dependence of CO emission on metal abundance is still uncertain, the data does suggest a similar relationship between α_{gal} and A_{gal} (Figure 9 of Bolatto et al. (2013)).

We estimated the metal masses for the galaxies in the sample using observations of the following tracers: carbon atoms (C I), carbon monoxide molecules (CO) and dust grains, with calibration factors $\alpha_{\text{C I}}$, α_{CO} and α_{dust} , respectively. We used the calibration factors from Dunne et al. (2022), which was the first attempt to calibrate all three calibration factors simultaneously. The values we assume are $1/\alpha_{850\mu\text{m}} = 6.9 \times 10^{12} \text{ W Hz}^{-1} \text{ M}_{\odot}^{-1}$ for the dust, $\alpha_{\text{CO}} = 4.0 \text{ M}_{\odot} (\text{K km s}^{-1} \text{ pc}^2)^{-1}$ for the CO $J = 1 - 0$ line,§ and $\alpha_{\text{C I}} = 17 \text{ M}_{\odot} (\text{K km s}^{-1} \text{ pc}^2)^{-1}$ for the C I $J = 1 - 0$ line. We assume the uncertainties in the calibration factors $\alpha_{850\mu\text{m}}$, α_{CO} and $\alpha_{\text{C I}}$ are 31 per cent, 39 per cent and 19 per cent respectively, based on the values estimated in their paper.

We restricted ourselves to observations that are least likely to be affected by systematic uncertainties. We therefore used observations of atomic carbon in the C I $J = 1 - 0$ line but not in the C I $J = 2 - 1$ line because of the recent evidence of subthermal excitation, which leads to large uncertainties in ISM masses estimates from this line (Papadopoulos et al. 2022). We used observations of carbon monoxide in the $J = 1 - 0$ and $J = 2 - 1$ lines but not in the higher J lines because the ratio of the line flux for these lines to the line flux for the $J = 1 - 0$ line, on which the calibration is based, depends strongly on the temperature of the gas. We estimated a line flux for the $J = 1 - 0$ line from the line flux in the $J = 2 - 1$ line using the flux ratio $\text{CO } 2 - 1 / 1 - 0 = 2.97 \pm 0.61$, which we derived from a study of carbon monoxide in a large sample of ultraluminous infrared galaxies (Papadopoulos et al. 2012).

We only used dust as a tracer if there was an observation close in rest-frame wavelength to $850 \mu\text{m}$, the wavelength at which the dust method is calibrated (Dunne et al. 2022), which in practice mostly meant observations in ALMA Band 3. We found unpublished observations in the ALMA archive for three galaxies, and we measured new flux densities for these, which are given in Table 2. Where there continuum observations at many wavelengths (Reuter et al. 2020) we fitted a modified blackbody ($F_{\nu} \propto B_{\nu} \nu^{\beta}$) to the flux densities at wavelengths $\geq 500 \mu\text{m}$, using a single dust temperature and a dust emissivity index $\beta = 2$. The advantage of estimating the dust temperature from only long-wavelength flux measurements is that the estimate should be closer to the mass-weighted dust temperature; the inclusion of flux measurements on the short-wavelength side of the blackbody peak biases the estimate towards the luminosity-weighted dust temperature (Eales et al. 1989). Our estimated dust temperatures for these galaxies are listed in Table 3 and they support the argument that the mass-weighted dust temperature, even for galaxies with very high star-formation rates, is $\approx 25 \text{ K}$ (Scoville et al. 2016). For these galaxies, we have estimated the rest-frame flux density at $850 \mu\text{m}$ from the best-fitting modified blackbody. For the galaxies for which there is only a flux measurement at a single wavelength, we estimated the rest-frame flux density at $850 \mu\text{m}$ from this measurement and a modified blackbody with a dust temperature of 25 K and $\beta = 2$.

Where necessary we corrected the line and continuum fluxes for the gravitational magnification factors given in Table 1. We have estimated errors on our metal masses by adding the following errors in quadrature: the error on the calibration factor (see above), the error on the flux of the tracer and, where applicable, the errors in the gravitational magnification factor and in the CO $2 - 1 / 1 - 0$ line ratio. All the galaxies in the sample have observations of at least one tracer, 10 have observations of two tracers, and seven have observations of all three.

3.2 Corrections for the Cosmic Microwave Background

At these redshifts, the cosmic microwave background (CMB) can have a large effect on submillimetre and radio observations, leading to underestimates in both line and continuum flux measurements. We have made corrections to the line and continuum fluxes using the method in [da Cunha et al. \(2013\)](#). In this work we estimate metal masses both with and without a correction for the CMB because of the potential for errors introduced by the assumptions necessary in making this correction.

For optically thin radiation, which is the case for the dust continuum radiation at long wavelengths and the $\text{C I } J = 1 - 0$ line ([Harrington et al. 2021](#); [Papadopoulos et al. 2022](#)), the CMB corrections only depend on the temperature of the dust and the excitation temperature of the gas, respectively. We corrected the continuum flux densities for each galaxy on the assumption that the temperature of the dust is 25 K (§3.1). We then estimated the rest-frame 850- μm flux density from the corrected flux densities using the procedure described in §3.1.

The excitation temperature of the $\text{C I } 1 - 0$ line for SMGs is ≈ 25 K ([Papadopoulos et al. 2022](#)), very similar to our estimates of the dust temperature (§3.1), which is what one would expect if the dust temperature and kinetic temperature are the same and the gas is in local thermodynamical equilibrium. We have made the assumption that the dust temperature and excitation temperatures are the same and calculated the CMB corrections using the equation for the increase in dust temperature caused by the CMB given by [da Cunha et al. \(2013\)](#) (equation 12 in their paper).

The corrections for the $\text{CO } J = 1 - 0$ and $J = 2 - 1$ lines are not so obvious since the lines are optically thick, which means the corrections should depend on the opacity of the gas as well as on its temperature ([da Cunha et al. 2013](#)). The uncertainties in the corrections from the inclusion of opacity are so large that we decided not to try to include opacity but to apply the same method as for the optically-thin C I line. Our CMB corrections for the CO lines therefore show the possible size of the effect of the CMB, but the actual size of the correction for these lines is very uncertain.

3.3 Results

Table 3 lists our estimates of the mass of metals using the three independent tracers, with and without a correction for the CMB. The results are shown in Figure 1. The figure shows that there is very good agreement between the masses calculated using the different tracers. For nine out of 10 galaxies, the different mass measurements are consistent within the errors. The only exception is SPT0345-47, for which the estimates from CO and dust are in very good agreement, but both are higher than the 3σ upper limit from the $\text{C I } 1 - 0$ observation.

The line at the bottom of each panel shows an estimate of the mass of metals in the molecular phase of the ISM in the Galaxy ($1.3 \times 10^7 M_\odot$), which we have calculated from an estimate of the mass of molecular gas in the Galaxy of $\approx 1.1 \times 10^9 M_\odot$ ([Yin et al. 2009](#)) and estimates of the gas-to-dust ratio (167.2) and of the fraction of metals in dust (0.52) from [Roman-Duval et al. \(2022\)](#). The mass of metals in the ISM in these high-redshift galaxies is ≈ 100 - 1000 times greater than in the molecular gas in the Galaxy today.

Since it seems likely that the SMGs are the ancestors of present-day massive early-type galaxies (§1), it is interesting to compare the masses of metals for the two populations. A useful low-redshift benchmark is the *Herschel* Reference Survey (HRS), which contains the galaxies with the highest stellar masses in a volume of space that

includes the Virgo Cluster ([Boselli et al. 2010](#); [Eales et al. 2017](#)). Since most of the metals in an early-type galaxy are contained in the stars, we have estimated the metal mass for the HRS early-type galaxies from estimates of their stellar masses ([De Vis et al. 2017](#)) and a stellar metal abundance of $\log_{10}(Z/Z_\odot) = 0.3$, appropriate for the galaxies with the highest masses ([Gallazzi et al. 2005](#)). In the figure, the purple horizontal band shows the range of metal mass for the HRS early-type galaxies, from the one with the largest stellar mass down to the one with the tenth largest stellar mass. When the correction for the CMB is included (lower panel), the SMGs contain a mass of metals very similar to that in their probable descendants in the universe today.

3.4 Limitations of the Method

We have used the calibration factors from [Dunne et al. \(2022\)](#), but the values for all three calibration factors are very similar to the other recent best estimates in the literature. Our value for $\alpha_{\text{CO}} = 4.0 M_\odot (\text{K km s}^{-1} \text{ pc}^2)^{-1}$ is very similar to the value adopted in the latest big review article on the subject: $\alpha_{\text{CO}} = 4.36 \pm 0.9 M_\odot (\text{K km s}^{-1} \text{ pc}^2)^{-1}$ ([Tacconi et al. 2020](#)). It is lower than the value of $\alpha_{\text{CO}} = 6.5 M_\odot (\text{K km s}^{-1} \text{ pc}^2)^{-1}$ adopted by [Scoville and collaborators \(Scoville et al. 2016\)](#) but adopting this value would make the metal masses of the galaxies even higher. Our value for the calibration factor for the dust emission ($1/\alpha_{850\mu\text{m}} = 6.9 \times 10^{12} \text{ W Hz}^{-1} M_\odot^{-1}$) is very similar to the value adopted in [Scoville et al. \(2016\)](#) ($1/\alpha_{850\mu\text{m}} = 6.2 \times 10^{12} \text{ W Hz}^{-1} M_\odot^{-1}$). Our value for the calibration factor for atomic carbon ($\alpha_{\text{CI}} = 17.0 M_\odot (\text{K km s}^{-1} \text{ pc}^2)^{-1}$) is also similar to the value found in the most comparable large study ([Heintz & Watson 2020](#)): $\alpha_{\text{CI}} = 21.4^{+13}_{-8} M_\odot (\text{K km s}^{-1} \text{ pc}^2)^{-1}$.

Although our method should still give the correct result if the metal abundance of the ISM in the SMG is different from that of the ISM in the Galaxy, it still relies on the assumption that there are no differences in the physics/chemistry of the ISM in the SMG from that in the ISM of the Galaxy that lead to changes in the values of the calibration factors. We will look at this issue in the next section, in which we show that there is evidence that the calibration factors for the SMGs are lower than the standard values. But we will argue that this is probably caused by changes in the metal abundance rather than changes in the physics/chemistry of the ISM. If this is so, our estimates of the metal mass are unaffected.

4 WHAT DO THE DYNAMICAL MASSES TELL US?

4.1 Estimates of the Masses

The evidence that the gas in the SMGs lies in a cold rotating disk is two-fold. First, the SMGs all have velocity profiles (velocity versus radius) that are very similar to the velocity profiles of rotating disk galaxies in the universe today. Second, the galaxies mostly have ratios of $v_{\text{rot}}/\sigma > 10$, in which v_{rot} is the rotational velocity of the gas and σ is its velocity dispersion. Such a high ratio suggests that gravity in the galaxy is being balanced by centripetal force rather than by the internal pressure provided by the spread in stellar velocities. All 13 galaxies have published estimates of their dynamical masses, which are listed in Table 4. In all cases, these have been obtained using modelling packages such as 3DBarolo ([Di Teodoro & Fraternali 2015](#)), which make it possible to vary the velocities in concentric rings around the centre of the galaxy, and also the position of the

Table 3. The Mass of Metals

Source	Metal masses with no CMB correction ($10^9 M_\odot$)			Metal masses with CMB correction ($10^9 M_\odot$)			T_d^a (K)	Z (Z_\odot)	References
	CO	C I	Dust	CO	C I	Dust			
SPT0113-46	0.79 ± 0.36	1.09 ± 0.30	0.58 ± 0.21	1.50 ± 0.69	1.70 ± 0.47	1.01 ± 0.37	19.8	0.99 ± 0.24	2,3,4
ALESS073.1	1.20 ± 0.60	...	2.42 ± 0.85	2.53 ± 1.26	...	3.93 ± 1.38		2.5 ± 0.9	1,5
SPT0345-47	2.58 ± 1.18	...	2.14 ± 0.79	4.95 ± 2.28	...	3.86 ± 1.42	32.7	6.1 ± 2.0	2,3,4
SPT0418-47	0.44 ± 0.21	0.58 ± 0.18	0.22 ± 0.08	0.81 ± 0.34	0.91 ± 0.28	0.39 ± 0.15	18.4	0.73 ± 0.20	2,3,4
SPT0441-46	0.91 ± 0.43	1.21 ± 0.55	0.92 ± 0.34	1.84 ± 0.80	2.00 ± 0.91	1.76 ± 0.66	21.9	2.7 ± 0.8	2,3,4
DLA0817g	1.05 ± 0.55	1.96 ± 1.03		1.5 ± 0.9	6
SDP81	1.61 ± 0.69	...	1.39 ± 0.48	2.53 ± 1.15	...	1.76 ± 0.61		3.3 ± 1.1	1,7
AZTEC/C159	1.31 ± 0.63	3.80 ± 1.84		1.5 ± 1.2	8
J1000+0234	2.38 ± 0.85	3.60 ± 1.29		0.94 ± 0.35	1
GN20	10.40 ± 5.54	...	5.47 ± 2.03	18.63 ± 9.89	...	7.73 ± 2.87		0.96 ± 0.38	9,10
ID141	3.68 ± 1.61	3.91 ± 1.08	4.67 ± 1.51	7.59 ± 3.33	5.77 ± 2.52	6.95 ± 2.25		4.9 ± 1.9	11
SPT2132-58	1.99 ± 0.91	1.30 ± 0.54	2.47 ± 0.93	4.26 ± 1.95	2.30 ± 0.97	5.13 ± 1.94	25.3	5.7 ± 1.9	2,3,4
SPT2146-55	1.79 ± 0.85	3.57 ± 1.17	1.87 ± 0.70	3.68 ± 1.72	6.02 ± 1.97	3.66 ± 1.36	26.5	12.9 ± 3.6	2,3,4

Notes: ^aDust temperature obtained by fitting a modified blackbody to the flux measurements at wavelengths $\geq 500 \mu\text{m}$ (see text).

References: 1: This paper; 2: Reuter et al. (2020); 3: Aravena et al. (2016); 4: Bothwell et al. (2017); 5: Coppin et al. (2010); 6: Neeleman et al. (2020); 7: Dye et al. (2015); 8: Jiménez-Andrade et al. (2018); 9: Hodge et al. (2012); 10: Daddi et al. (2009); 11: Dye et al. (2022).

centre and the inclination and position angle of the disk, until the model provides a good fit to the spectroscopic data.

For six of the 13 galaxies, the authors of the mass estimate have made an explicit correction for the effect of the stellar pressure, the ‘asymmetric drift’. In the other studies, the authors have simply assumed it is negligible because of the high ratio of v_{rot}/σ . For each of the galaxies, we have used the data in the original papers to estimate the relative contributions of the asymmetric drift and the centripetal force, and where necessary made a correction to the published masses (Appendix A). For all but two galaxies the correction to the mass is ≤ 10 per cent.

The original papers sometimes list separate estimates of the baryonic and non-baryonic masses (we list the former in Table 4). In order to check that the attempt to model separately the distribution of the baryonic and non-baryonic mass has not led to systematic errors in the mass estimates - as well as to check that there are no other hidden systematic errors in the original analysis - we have made our own estimates of the dynamical masses from the velocity profiles and the estimates of the galaxy inclination in the original paper.

We have made estimates of the mass from the equation:

$$M_{\text{tot}} = \frac{v^2 r}{G \sin(i)^2} \quad (3)$$

in which v is the rotational velocity of the gas at a distance r from the centre of the galaxy and i is the estimate of the inclination of the disk. We have made a correction to these estimates for the effect of asymmetric drift (Appendix A). Equation 3 gives the correct mass interior to r if the density distribution is spherically symmetric. If the density is not spherically symmetric our mass estimates will be too high (Walter et al. 1997), by roughly 40 per cent if the mass is distributed in a razor-thin exponential disk¹. We calculated errors on the mass estimates by combining the errors in velocity and inclination. Table 4 lists our mass estimates and the distance from the centre of the SMG at which we made the estimate.

¹ Bovy et al. 2022, *Dynamics and Astrophysics of Galaxies*, galaxies-book.org, accessed 7/4/2022

The published mass estimates and own estimates are in good agreement for 10 out of the 13 galaxies, which agrees with the evidence that non-baryonic matter is negligible in the central regions of high-redshift galaxies (Genzel et al. 2017). For the three galaxies where there is a significant discrepancy, our mass estimate is higher than the published mass by a factor of 1.6 for ALESS073.1, by a factor of 2.1 for SPT0418-47 and by a factor of 1.5 for SPT0441-46.

4.2 The ISM Mass Versus Dynamical Mass

We estimated the mass of the ISM in each galaxy using equation (1) rather than equation (2) but otherwise followed the procedure described in Section 3.1, which means our ISM mass estimates are equal to the metal mass estimates in Table 3 multiplied by the gas-to-metal ratio (86.9). Since the dynamical masses we have measured ourselves are slightly larger than the ones in the literature, and therefore place a less stringent upper limit on the ISM mass, to be conservative we have used our mass estimates rather than the published ones.

Ideally, we would compare the dynamical mass with an ISM mass estimate made within the radius used to estimate the dynamical mass. This is possible for the observations of the dust, for which there are high-resolution observations which show the emission is coming from within the radius listed in Table 4 (Daddi et al. 2009; Dye et al. 2015; Spilker et al. 2016; Dye et al. 2022)). However, most of the CO and C I observations (Aravena et al. 2016; Bothwell et al. 2017) do not have enough resolution to show whether the CO and C I emission is coming from within the region covered by the dynamical analysis. There is a high-resolution map of C I 1–0 for one galaxy (Dye et al. 2022) and a high-resolution map of CO for one galaxy (Hodge et al. 2012), and in both cases the line emission from the tracer comes from the region covered by the dynamical analysis. Furthermore, by detailed radiative modelling of multiple CO and C I lines from 24 high-redshift SMGs, Harrington et al. (2021) concluded that the emission in these lines is typically from a region within 3 kpc of the centre of the galaxy, very similar for most of the galaxies to the radius of the region covered by the dynamical analysis (Table 4). Nevertheless, we cannot say this for certainty for most of the galaxies that the C I and CO emission is confined to the region covered by the

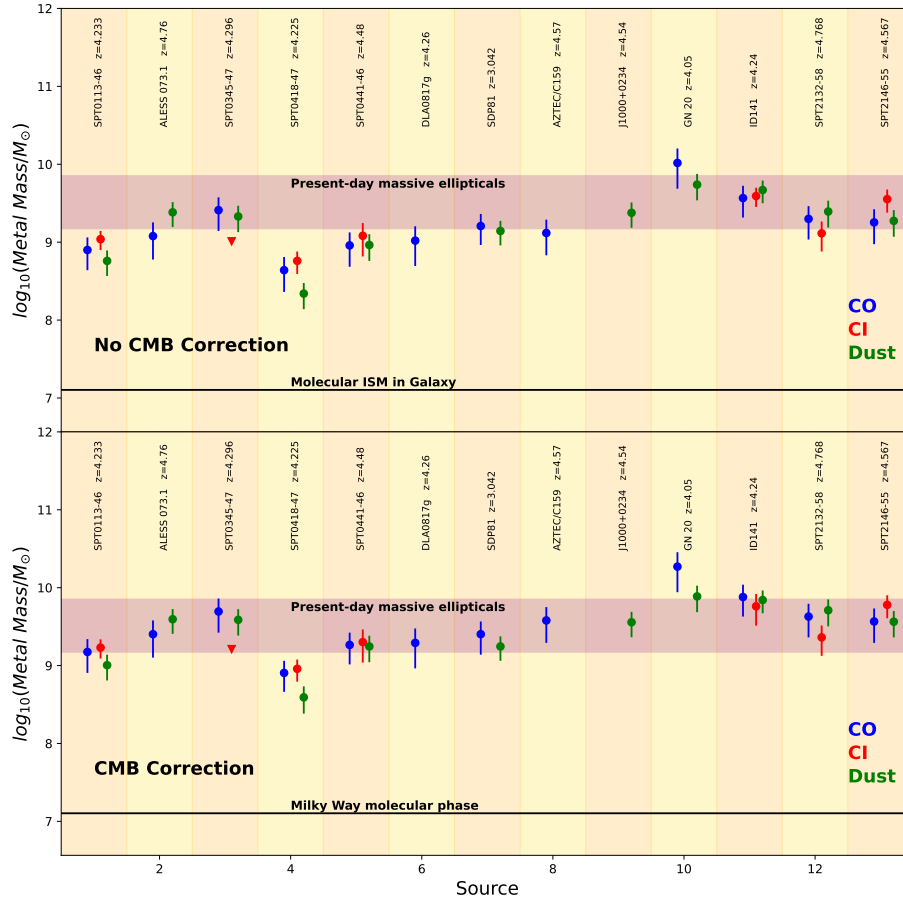


Figure 1. Estimates of the metal mass in the 13 SMGs estimated from CO lines (blue), the C I 1 – 0 line (red) and dust continuum emission (green). The upper panel shows the estimates without a correction for the effect of the CMB, the lower panel the estimates after this correction has been made. The horizontal line shows an estimate of the mass of metals in the molecular gas in the Galaxy today (see text). The horizontal purple band shows an estimate of the range of metal mass for the most massive early-type galaxies in the universe today (see text).

Table 4. Dynamical Masses

Source	Mass from literature ($10^{11} M_{\odot}$)	Our Mass estimate ($10^{11} M_{\odot}$)	Radius (kpc)	Correction for asymmetric drift (percentage)	Reference
SPT0113-46	1.1 ± 0.1	0.93 ± 0.13	3.2	1.0	Rizzo et al. (2021)
ALESS073.1	0.55 ± 0.13	0.89 ± 0.19	3.5	5.0	Lelli et al. (2021)
SPT0345-47	0.40 ± 0.03	0.48 ± 0.08	3.0	8.2	Rizzo et al. (2021)
SPT0418-47	0.25 ± 0.02	0.53 ± 0.08	3.5	2.1	Rizzo et al. (2020)
SPT0441-46	0.32 ± 0.02	0.48 ± 0.09	2.0	1.4	Rizzo et al. (2021)
DLA0817g	0.91 ± 0.29	0.90 ± 0.19	4.2	26	Neelman et al. (2020)
SDP81	0.38 ± 0.06	0.41 ± 0.08	1.5	9.8	Dye et al. (2015)
AZTEC/C159	1.4 ± 0.7	1.8 ± 1.1	3.0	0.2	Fraternali et al. (2021)
J1000+0234	2.3 ± 0.3	2.7 ± 0.3	4.0	0.8	Fraternali et al. (2021)
GN20	6.4 ± 2.8	6.3 ± 1.5	7.0	18	Hodge et al. (2012)
ID141	1.0 ± 0.5	0.95 ± 0.29	2.0	2.0	Dye et al. (2022)
SPT2132-58	0.39 ± 0.04	0.38 ± 0.08	4.0	1.3	Rizzo et al. (2021)
SPT2146-55	0.22 ± 0.02	0.23 ± 0.04	2.7	2.0	Rizzo et al. (2021)

dynamical analysis. We discuss the possibility that there are halos of molecular gas around these galaxies, and its effect on our comparison of the dynamical and ISM masses, in §6.1.

Figure 2 shows the comparison between the dynamical and ISM mass. The dynamical mass is a measure of the total mass, which is the sum of the masses of all the galaxy's components: gas, stars, and non-baryonic matter. But Figure 2 shows that for many of the galaxies the ISM mass estimate is actually higher than the estimate of the total mass. This paradox has been spotted many times before when CO has been used as a tracer, but the figure shows that there is the same problem when C I and dust are used. There is, of course, the caveat that, as we noted above, for many of the galaxies we cannot be sure that the emission from the tracer is from within the region covered by the dynamical analysis, but we note that the discrepancies when dust is used as a tracer are just as large as for the other two tracers. Moreover, the galaxy for which there is a high-resolution map in C I 1-0, ID141 (Dye et al. 2022), is one of the best examples of this paradox.

4.3 A Possible Solution of the Paradox

This paradox has been noted many times before in papers in which CO has been used to estimate the mass of the ISM. Our results show that the same problem is present when carbon atoms and dust grains are used. Unless the assumptions used in the dynamical estimates are completely wrong, or the emission from the tracer is mostly from outside the region covered by the kinematic observations (§4.2), the only way to make the ISM masses consistent with the dynamical masses is to reduce the values of the three calibration factors.

A crucial point to note when thinking about this issue is that the good agreement between the ISM mass estimates made with the different tracers implies that if the calibration factors are lower for an SMG than the values we have assumed, which are ultimately based on observations in the Galaxy (Dunne et al. 2022), all three calibration factors must be lower by a similar factor. This conclusion is supported by the analysis in Dunne et al. (2022) of 407 galaxies in the redshift range $0 < z < 5$. By examining the ratios of the luminosity of the emission from the three tracers, these authors concluded that there was no difference in the ratios of the calibration factors between normal galaxies and galaxies with very high star-formation rates and also between SMGs at $z < 3$ and $z > 3$. These results strongly suggest that if the values of the calibration factors for the SMGs are different from the standard values, they must all be different by a similar factor.

There are two obvious reasons why the calibration factors for the SMGs might be lower than the values estimated from observations of the ISM in the Galaxy. The first is that physical/chemical/structural differences in the ISM of a high-redshift SMG relative to the ISM in the present-day Galaxy might easily lead to changes in the calibration factors. This has been the explanation that has always been favoured before when the discrepancy between the dynamical masses and the ISM masses estimated from CO observations has been noticed. This is quite a reasonable supposition because the hundred-fold difference in star-formation rates between an SMG and the Galaxy might easily lead to differences in the structure, physics or chemistry of the ISM.

The observational evidence that α_{CO} is lower in a galaxy with a high star-formation rate is, however, very slight, being based almost entirely on a study of CO in the nuclei of low-redshift ultra-luminous infrared galaxies (ULIRGs) (Downes & Solomon 1998). These authors argued that because of the strong shear in the velocity field in the central regions of these galaxies, where most of the CO is found, the CO emission must be from a moderate-density warm intercloud

medium rather than from self-gravitating clouds, as in the Galaxy. They estimated a value for α_{CO} lower than the standard value by a factor of ≈ 5 . The star-formation rates of the SMGs are similar to those of the ULIRGs, so it has always seemed plausible that the values of α_{CO} might be lower for them as well, although the ISM of an SMG is distributed over a much larger region than the ISM in a ULIRG, over which there is much less shear in the velocity field (Dye et al. 2015, 2022). Very recently, however, in the first comprehensive multi-line investigation of CO in SMGs, Harrington et al. (2021) estimated a value of α_{CO} for these objects very similar to the standard value. They concluded that much of the CO in SMGs is in warm dense gas, which would have been missed by the observations in low-J CO transitions, which were the ones used to observe the ULIRGs (Downes & Solomon 1998). With only observations of the SMGs in the low-J CO transitions, they concluded that they would have estimated a value of α_{CO} similar to that for the ULIRGs.

Nevertheless, it seems likely that the ISM in a high-redshift SMG is different in some ways from the ISM in the Galaxy, and it is easy enough to think of differences that might lead to changes in the calibration factors. The problem with this explanation is that it is difficult to think of differences that might lead to all three calibration factors being changed by the same factor. Differences in the spatial and temperature distribution of the ISM might lead to a change in α_{CO} ; differences in the sizes, structure or composition of the dust grains might lead to a change in α_{dust} ; and the high star-formation rate in an SMG would probably lead to a higher density of cosmic rays than in the Galaxy, which would lead to different proportions of carbon monoxide and atomic carbon, which might lead to a change in $\alpha_{\text{C I}}$ (Dunne et al. 2022). Therefore, it is easy enough to think of differences that would lead to changes in the calibration factors. However, since the emission from each tracer depends on such different properties of the ISM, it seems very unlikely that these differences would lead to the three calibration factors all being reduced and being reduced by a similar factor.

The alternative explanation is that the metal abundance of the ISM in the SMGs is higher than in the Galaxy today. This would also provide a natural explanation of why the three calibration factors change by similar amounts. As long as there is no change in the relative abundances of different elements, the optically-thin C I and dust emission are directly proportional to the metal abundance of the ISM, which implies that $\alpha_{\text{C I}}$ and α_{dust} are inversely proportional to metal abundance. The relationship between the optically-thick CO emission and metal abundance is more uncertain, but a compilation of the data is consistent with a similar relationship (Bolatto et al. 2013) (see their Figure 9). A higher metal abundance in SMGs would therefore be a natural explanation of why the calibration factors are lower by a similar factor.

For the rest of this paper, we assume that the second explanation is the correct one. We cannot rule out the first explanation, but it does seem unlikely that changes in different aspects of the ISM should have conspired to produce very similar changes in the calibration factors. If we are wrong and the first explanation is the correct one, a decrease by a factor of X in the three calibration factors would mean that our estimates of the metal masses in §3 would also need to be reduced by a factor X.

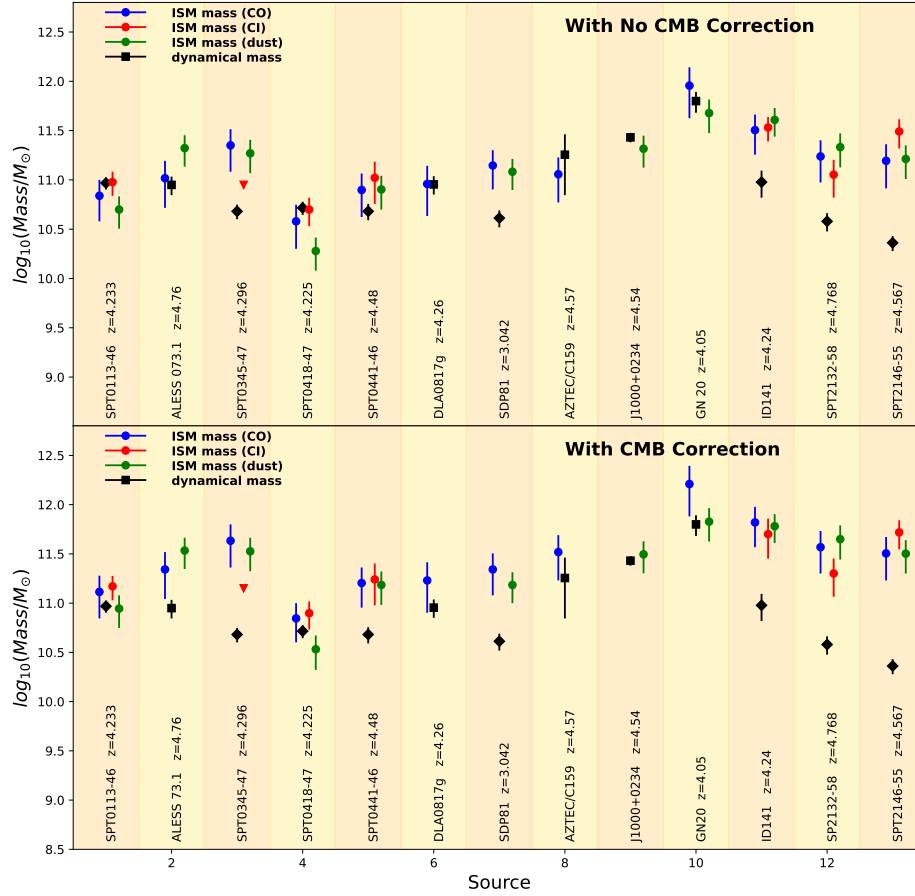


Figure 2. A comparison of the dynamical mass of each SMG with estimates of the mass of the ISM in the SMG made with three different tracers: carbon monoxide (blue), atomic carbon (red), dust grains (green). The estimate of the dynamical mass is shown by a black diamond if the source is gravitationally lensed and a black square otherwise. The upper panel shows the estimates of the ISM mass with no correction for the CMB, the lower panel the estimates after this correction has been made (see text).

4.4 Metal Abundances

We have estimated a lower limit to the metal abundance of each galaxy from the equation:

$$\frac{Z}{Z_{\odot}} = \frac{M_{\text{metals}}}{M_{\text{dyn}} \times 0.0142} \quad (4)$$

in which M_{metals} is the metal mass corrected for the effect of the CMB, M_{dyn} is the dynamical mass, and the number on the right-hand side is the bulk metal fraction of the Sun (Asplund et al. 2009). Our estimates of Z , which range from $0.9Z_{\odot}$ to $12.9Z_{\odot}$, are listed in Table 3 and a histogram of the values is shown in Figure 3.

5 METALS INSIDE AND OUTSIDE GALAXIES - CHEMICAL EVOLUTION MODELS

Such high metal masses and metal abundances at such early times might be surprising because there would have been much less time

to make the metals. We have used two chemical-evolution models to investigate the cause of these high values. The first is the widely used gas-regulation model (Lilly et al. 2013; Peng & Maiolino 2014). In this model, there is a flow of gas from the intergalactic medium into the galaxy, and there is also an outflow with a rate proportional to the galaxy's star-formation rate, which leads eventually to the mass of the ISM reaching an equilibrium value. The mass of metals that is produced in this model depends on the strength of the outflow and the form of the stellar initial mass function (IMF).

The gas-regulation model is based on the ‘instantaneous recycling approximation’, in which it is assumed that all the metals produced by a newly formed population of stars are made the moment the stars are born and immediately released into the ISM. This assumption is likely to be a particularly poor one for SMGs because of their very short gas depletion times (Dye et al. 2015, 2022). We have therefore also included the predictions of a model that does not include this assumption, which we constructed to model the evolution of one of the galaxies in our sample (Dye et al. 2022). This model also

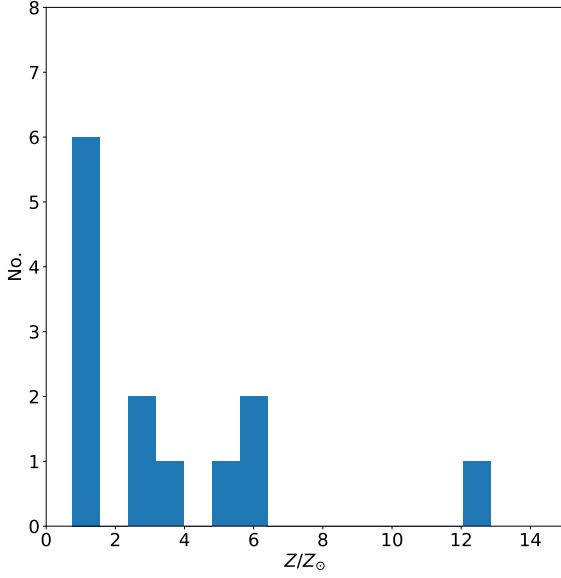


Figure 3. Estimates of the lower limit on the metal abundance for the 13 galaxies (§4.4).

includes more realistic inflows and outflows and takes account of the dependence of stellar yields on metal abundance.

5.1 The Gas-Regulation Model

In this model, there is an outflow with a rate equal to a constant (Λ) times the galaxy’s star-formation rate, which leads to the mass of the ISM eventually reaching an equilibrium value (hence the term ‘gas regulation’). We use the analytic formalism of [Peng & Maiolino \(2014\)](#), which makes it possible to follow the evolution of a galaxy from $t = 0$ to $t \gg \tau_{\text{eq}}$, when the galaxy asymptotically approaches an equilibrium state. In this equilibrium state, the gas mass, the metal abundance of the gas and the mass of metals in the gas are constants, although the fraction of the mass of the galaxy that consists of stars continues to climb as new stars are made out of gas.

The equilibrium time, τ_{eq} is given by

$$\tau_{\text{eq}} = \frac{\tau_{\text{dep}}}{1 - R + \Lambda} = \frac{1}{\epsilon(1 - R + \Lambda)} \quad (5)$$

in which τ_{dep} is the depletion time (the ratio of the gas mass to the star-formation rate), ϵ is the inverse of this (the star-formation efficiency), and R is the fraction of the mass of a cohort of newly formed stars that is eventually returned to the ISM, which in the instantaneous recycling approximation happens immediately. The equilibrium time therefore depends on conditions in a particular galaxy, and so we express the time dependence of our models in units of the equilibrium time, so the models are applicable to all the galaxies in our sample.

We have used the following equations taken directly from [Peng & Maiolino \(2014\)](#):

$$M_{\text{gas}} = \frac{\Phi}{\epsilon(1 - R + \Lambda)} \left(1 - e^{-\frac{t}{\tau_{\text{eq}}}} \right) \quad (6)$$

$$M_{\text{star}} = \frac{\Phi}{\epsilon} \frac{1 - R}{(1 - R + \Lambda)^2} \left[\frac{t}{\tau_{\text{eq}}} - \left(1 - e^{-\frac{t}{\tau_{\text{eq}}}} \right) \right] \quad (7)$$

$$Z_{\text{gas}} = \frac{y}{1 - R + \Lambda} \left(1 - e^{-\frac{t}{\tau_{\text{eq}}}} \right) \left[1 - e^{-\left(\frac{t}{\tau_{\text{eq}}(1 - e^{-\frac{t}{\tau_{\text{eq}}}})} \right)} \right] \quad (8)$$

In these equations, y is the yield, the mass of metals produced by one solar mass of stars, and Φ is the rate at which gas is flowing onto the galaxy. We can combine equations (6) and (8) to get an estimate of the total mass of metals in the ISM:

$$M_{\text{metals}} = Z_{\text{gas}} M_{\text{gas}} \quad (9)$$

We then combine equations (6), (7) and (9) to calculate the ratio of the metal mass to the total mass ($M_{\text{gas}} + M_{\text{star}}$). Neither this ratio nor the metal abundance of the ISM (equation 8) depend on the values of Φ or ϵ but they do depend on the values of R , y and Λ . The first two of these depend on the choice of the IMF.

5.2 A Bespoke SMG Model

The instantaneous recycling assumption may be particularly poor for SMGs because of their very short gas-depletion and dynamical times ([Dye et al. 2015, 2022](#)). We have therefore also used a chemical evolution model we developed for the $z=4.24$ submillimetre galaxy ID141, which does not include this assumption and which incorporates the lifetimes of the stars that make the metals ([Dye et al. 2022](#)). We refer the reader to our earlier paper for more details of the model but, in brief, the galaxy starts as a cloud of gas with no heavy elements, with the gas then being converted into stars using an assumed IMF and star-formation history. Outflows of gas and metals are based on prescriptions of feedback from stars and active galactic nuclei, and the model includes inflows via accretion from the cosmic web. Stars eject gas, metals and dust in each generation based on prescriptions for the stellar yield of low-mass ([van den Hoek & Groenewegen 1997](#)) and high-mass stars ([Maeder 1992](#)) and for the remnant mass function ([De Vis et al. 2021](#)).

5.3 Results

We have considered four different forms for the IMF. The first two are the commonly used Chabrier and Salpeter IMFs. The other two are top-heavy IMFs in which there is a higher proportion of high-mass stars. One of these was proposed to explain the dynamics of low-redshift elliptical galaxies ([Cappellari et al. 2012](#)), the other to explain the observations of isotopologues of carbon monoxide in four SMGs ([Zhang et al. 2018](#)). We have estimated the values of the return fraction, R , and the yield, y , for each IMF from a compendium of stellar yields ([Nomoto et al. 2013](#)). The values are listed in Table 5.

The prediction of both models for the ratio of metal mass to total mass (gas plus stars) versus time are shown in Figure 4 and the predictions for metal abundance versus time in Figure 5. Time is plotted in units of the equilibrium time, a key parameter of the gas-regulation model, along the top of each figure. To give an impression of the timescales, we have calculated the value of τ_{eq} in years using a Chabrier IMF and the properties of the galaxy ID141 ([Dye et al. 2022](#)), and then plotted time in the usual units along the bottom of

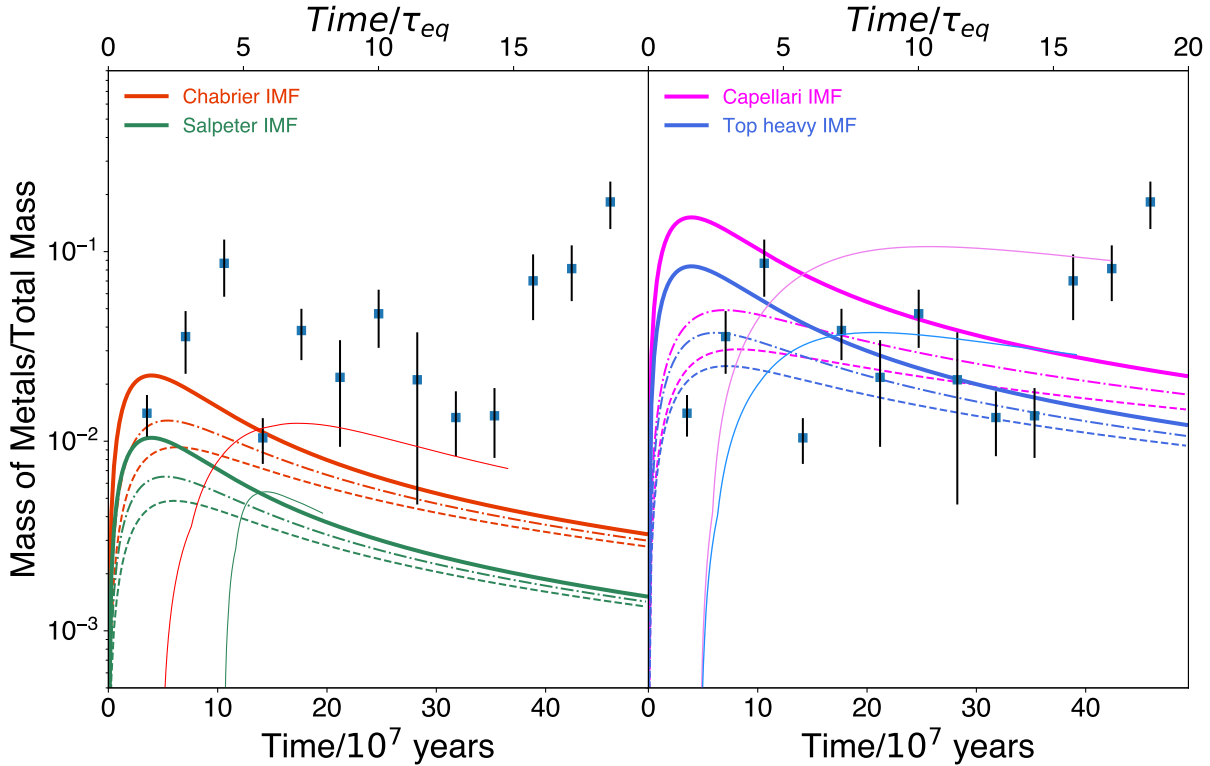


Figure 4. The ratio of the mass of metals in the ISM to the total mass of the galaxy plotted against cosmic time. Since we do not know the ages of the SMGs, our estimates of this ratio are plotted at arbitrary positions along the time axis. The thick lines show the predictions of the gas-regulation model, in which metals are instantaneously ejected into the ISM, the thin lines the predictions from a model that includes the delay in metal production from the lifetimes of the stars (see text). The different colours show the predictions for different IMFs, the left panel for two standard IMFs (Chabrier and Salpeter) and the right panel for two IMFs with a larger proportion of high-mass stars (Cappellari et al. 2012; Zhang et al. 2018) (key at top of each panel). The continuous, dot-dashed and dashed lines show the predictions for different outflow parameters: $\Lambda = 0, 1, 2$, respectively. Time is expressed in units of the equilibrium time used in the gas-regulation model along the top of the figure and in years along the bottom of the figure (see text).

the figures, although strictly this is only correct for one galaxy and one form of the IMF. We stopped the model based on ID141 (Dye et al. 2022) when it reached a stellar mass of $5 \times 10^{11} M_{\odot}$ when we assume an outflow clears the galaxy of its ISM (Romano et al. 2017). The left panel in each figure shows the predictions for the standard Chabrier and Salpeter IMFs and the right panels show the predictions for the top-heavy IMFs.

In Figure 4, we have plotted our estimates for the SMGs of the ratio of metal mass to total mass, which we assume is given by the dynamical mass. In Figure 5, we have plotted our estimates of the lower limits on the metal abundance. Since the ages of the galaxies are unknown, we have plotted our estimates in both figures at arbitrary points along the time axis.

Figure 4 shows that the predictions of both models are very similar, with the only difference being, as expected, that the ratio of metal mass to total mass peaks later for the model that includes a delay from stellar lifetimes. Nevertheless, even in this model, the peak is reached very early, only $\approx 2 \times 10^8$ years after the galaxy begins to form, much less than the time since the big bang at these redshifts.

The left-hand panel of Figure 4 shows that the predictions for the two standard forms of the IMF are too low compared with our estimates for the SMGs. The left-hand panel of Figure 5 shows that while it is possible to reproduce the observed metal abundance for a standard IMF and a closed-box model, this model seems unlikely given the evidence for outflows from star-forming galaxies in the

high-redshift universe (Spilker et al. 2018; Jones et al. 2019; Ginolfi et al. 2020; Veilleux et al. 2020).

The right-hand panels in both figures show that with a top-heavy IMF the predictions agree better with the observations. We note that although we don't know the ages of these galaxies, it seems likely that we are seeing them at an epoch at which the dust mass, and therefore the mass of metals in the ISM, was at close to its maximum value, simply because of the strong selection bias towards high dust masses for galaxies discovered in a submillimetre survey.

The curves in both figures for both sets of models are sensitive to the choice of input yields and the chosen remnant mass function (which in turn affects the return fraction R). Different stellar yield tables (Limongi & Chieffi 2018; Karakas et al. 2018), for example, can reduce the yield, y , and hence the metal abundance, Z_{gas} , by 20-30 per cent for the Cappellari IMF (Cappellari et al. 2012). This is not enough to affect the conclusions above.

5.4 The Metals in the Intracluster Gas

Our analysis shows that the SMGs contain very large masses of metals. There is plenty of evidence for massive outflows of gas from high-redshift star-forming galaxies (Spilker et al. 2018; Jones et al. 2019; Ginolfi et al. 2020; Veilleux et al. 2020). In this section, we will investigate whether the metal production in the SMGs might be a significant source of the metals in the intergalactic medium to-

Table 5. Our Assumptions About the Return Fraction and Yield^a

IMF	Yield (y)	Return Fraction (R)
Salpeter	0.023	0.24
Chabrier	0.040	0.38
Top-heavy (Cappellari et al. 2012)	0.088	0.80
Top-heavy (Zhang et al. 2018)	0.085	0.65

^aWe use the definition of yield in Peng & Maiolino (2014).

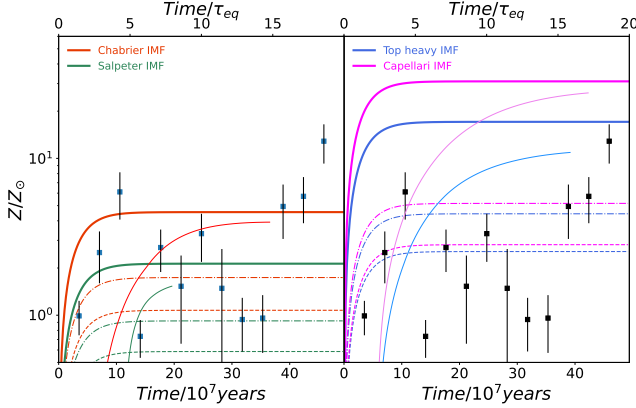


Figure 5. Metal abundance of the ISM plotted against cosmic time. Since we don’t know the ages of the SMGs, our estimates of the metal abundance are plotted at arbitrary positions along the time axis. The thick lines show the predictions of the gas-regulation model, in which metals are instantaneously ejected into the ISM, the thin lines the predictions of a model that includes the delay in the metal production from the lifetimes of the stars (see text). The different colours show the predictions for different IMFs, the left panel for two standard IMFs (Chabrier and Salpeter) and the right panel for two IMFs with a larger proportion of high-mass stars (Cappellari et al. 2012; Zhang et al. 2018) (key at top of each panel). The continuous, dot-dashed and dashed lines show the predictions for different outflow parameters: $\Lambda = 0, 1, 2$, respectively. Time is expressed in units of the equilibrium time used in the gas-regulation model along the top of the figure and in years along the bottom of the figure (see text).

day. As a test case, we will consider the long-standing conundrum that ≈ 75 percent of the metals in rich clusters of galaxies is in the intergalactic gas rather than in the galaxies themselves (Renzini & Andreon 2014), which previous models have not been able to explain (Loewenstein 2013; Renzini & Andreon 2014). The strong gravitational fields of clusters mean that any metals produced in a cluster should have stayed in the cluster. The clusters are dominated by early-type galaxies and the most likely ancestors of these galaxies are the SMGs (§1), and it therefore seems likely that the metals produced in the SMGs must have contributed at least in part to the metals found in the intracluster gas. We use the gas-regulation model to estimate how big a part this might have been.

We follow on from the exposition of the gas-regulation model in §5.1. On the assumption that the metal abundance in the outflowing gas is the same as in the ISM in the galaxy, the mass of metals ejected into intergalactic space is given by:

$$M_{\text{ejected metals}} = \int_0^{t_{\text{final}}} Z_{\text{gas}} \Lambda \text{SFR} dt \quad (10)$$

in which SFR is the star-formation rate, which is given by:

$$\text{SFR} = \frac{\Phi}{1 - R + \Lambda} (1 - e^{-\frac{t}{\tau_{\text{eq}}}}) \quad (11)$$

The predicted mass of metals that is incorporated in the stars within a galaxy is given by:

$$M_{\text{metals, stars}} = (1 - R) \int_0^{t_{\text{final}}} Z_{\text{gas}} \text{SFR} dt \quad (12)$$

The predicted metal abundance of the stars is then given by:

$$Z_{\text{stars}} = \frac{\int_0^{t_{\text{final}}} Z_{\text{gas}} \text{SFR} dt}{\int_0^{t_{\text{final}}} \text{SFR} dt} \quad (13)$$

In Figure 6, we have plotted on the y-axis the prediction of the model for the ratio of the mass of metals carried away in the outflow to the mass of the metals that is incorporated in the galaxy’s stars. The x-axis shows the model’s prediction for the final metal abundance of the stars (mass of metals divided by mass of stars). The former is given by the ratio of equations (10) and (12), the latter by equation (13). The former is independent of t_{final} and the latter is only weakly dependent on it - we have set its value to $20 \tau_{\text{eq}}$. There is evidence that the average value of Λ for the population of high-redshift star-forming galaxies lies between 1 and 2 (Ginolfi et al. 2020). We have plotted the predictions of the model for outflows with these values and for the four forms of the IMF.

Also plotted in Figure 6 are the rough observational targets for the model. The horizontal blue band shows the observed range of the metal ratio (mass of metals in cluster gas divided by mass of metals in the cluster galaxies) for present-day rich clusters (Renzini & Andreon 2014). The two vertical lines show solar metal abundance (Asplund et al. 2009) and a metal abundance of twice solar, typical of the most massive galaxies in the universe today (Gallazzi et al. 2005).

All the models predicts values that are roughly in the target area, which, given their simplicity, shows that outflows of metals from SMGs are at least a plausible source for the metals in the intracluster gas in present-day rich clusters.

6 DISCUSSION

6.1 The Observational Results

We have two main observational results: (1) the mass of metals in an SMG is very high, as large as the entire metal content of a massive low-redshift early-type galaxy; (2) the metal abundance is also very high, often well over the solar value. In this section, we will discuss the limitations of these results. In the following section we will discuss their implications for galaxy evolution.

The first result seems robust. It is based on the estimates of the calibration factors of Dunne et al. (2022), who made the first attempt to estimate all three calibration factors in a self-consistent procedure. Nevertheless, the values we have used are actually quite similar to the other recent estimates in the literature (§3.4). The comparison between the ISM mass estimates and dynamical mass estimates in Figure 2 implies that the true calibration factors for the SMGs must be lower than these values, but as long as this decrease is caused by an increase in the metal abundance rather than differences in the ISM that reduce all three calibration factors by a similar factor, our estimates of the metal mass are unaffected (§4.3). Since the

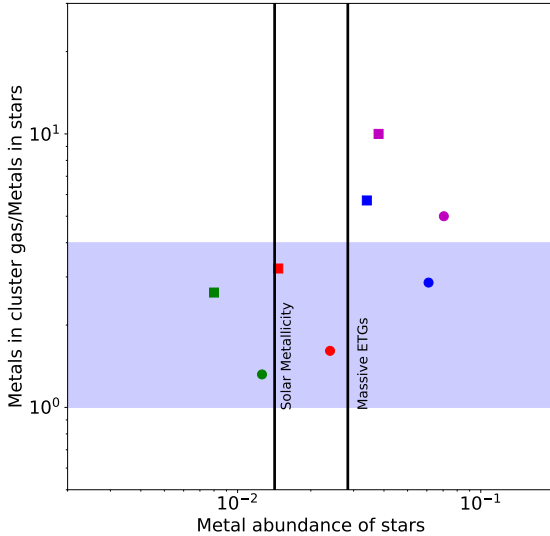


Figure 6. The ratio of the mass of metals ejected from a galaxy to the mass of metals in the galaxy’s stars plotted against the metal abundance of the stars. The coloured symbols show the prediction of the eight models: blue - top-heavy IMF (Zhang et al. 2018); red - Chabrier IMF; purple - top-heavy IMF (Cappellari et al. 2012); green - Salpeter IMF; circles - $\Lambda = 1$; squares - $\Lambda = 2$. The purple band shows the observed range of values for present-day clusters for the ratio of the mass of metals in the intracluster gas to the mass of metals in the galaxies (Renzini & Andreon 2014). The left-hand vertical line shows solar metal abundance (Asplund et al. 2009). The right-hand vertical line shows a metal abundance of twice solar, typical of the most massive galaxies in the universe today (§3.3).

calibration factors all depend on such different aspects of the physics and chemistry of the ISM, the latter explanation seems unlikely, but it is not impossible.

There are two causes for concern over the second result. The first is that it does rely on the dynamical masses being correct. We have made our own estimates of the dynamical masses from the published rotation curves, obtaining similar values to the ones in the literature, but both sets of masses are based on the assumption that the gas in these galaxies is distributed in a cold rotating disk. The velocity profiles for these galaxies do look remarkably like the rotation curves of present-day disk galaxies (see, for example, the beautiful velocity profile of SDP81 in Dye et al. (2015)), but it is possible that there may be an alternative explanation of these very disk-like velocity profiles.

A more immediate concern is that for the most of the CO and C I observations, we cannot be sure that the emission is from within the region traced by the dynamical analysis. There have been some recent claimed detections of molecular gas in the halos around high-redshift AGN (Jones et al. 2023; Scholtz et al. 2023). If some of the CO or C I emission is coming from halos around the SMGs, the conflicts between the ISM and dynamical masses would be less and the limits on the metal abundance weaker. To estimate the possible size of this effect, we can use the results of Scholtz et al. (2023), who used a stacking analysis to search for extended emission in the C I 2–1 line around extremely red quasars. They estimated average molecular masses of $10^{10.8 \pm 0.14} M_{\odot}$ and $10^{10.2 \pm 0.16} M_{\odot}$ for the galaxy and

halo components, respectively. If these proportions applied to the galaxies in our sample, our limits on the metal abundance of the SMGs would be lower by $\approx 20\%$, which would still require very high values of the metal abundance. It would leave unaffected our estimates of the total mass of metals, although the metals would be distributed over a larger region. An obvious way to test whether the emission from the CO and C I is confined within the region traced by the dynamical analysis would be future high-resolution observations with the JVLA in the low-J CO lines and with ALMA in the C I 1–0 line.

Our lower limits for the metal abundance in these galaxies are much higher than almost all the estimates of the metal abundance in high-redshift galaxies so far made with the JWST (Arellano-Córdova et al. 2022; Curti et al. 2023; Carnall et al. 2023; Heintz et al. 2022; Schaefer et al. 2022; Tacchella et al. 2022; Taylor et al. 2022). By good fortune, though, one of the galaxies in our sample already has a measurement of the metal abundance with the JWST: SPT 0418-47 (Peng et al. 2022). Using two of the standard methods from optical spectroscopy (N2 and S23), these authors estimated a metal abundance of $Z \sim 1.6Z_{\odot}$. Our lower limit for this galaxy is $Z > 0.58Z_{\odot}$, and so for this galaxy at least the two methods give consistent results.

6.2 Implications for Galaxy Evolution

We have shown that it is possible to reproduce the high values of the metal abundance in the SMGs with chemical evolution models (§5). In these models, the mass of metals in the ISM of an SMG is at its highest only $\sim 2 \times 10^8$ years after the galaxy begins to form, much less than the age of the universe at these redshifts. The values for the ratio of metal mass to total mass (Figure 4) and of the metal abundance (Figure 5) can be reproduced by the models as long as the IMF has a higher fraction of high-mass metal-producing stars than in the Galaxy. Our conclusion that the IMF in the SMGs is ‘top-heavy’ is supported by observations of isotopologues of CO in four SMGs, which can also only be explained by a top-heavy IMF (Zhang et al. 2018).

We have also used these models to show that the metals in outflows from the SMGs provide a plausible explanation of why such a large fraction of the metals in present-day clusters is found in the intracluster gas (§5.4). Figure 6 shows that this conclusion does not require a top-heavy IMF, since even models with standard IMFs do well at reproducing the proportions of the metals in the galaxies and the gas - the success of the models is due to the large metal masses and vigorous outflows of SMGs rather than the high values of the metal abundance, which is the observational result that requires a top-heavy IMF. Our model is, of course, a very simple model, which we have applied to SMGs with some of the highest star-formation rates known, which are likely to be the ancestors of only the most massive early-type galaxies in clusters. Present-day clusters contain galaxies with a wide range of stellar mass. A conclusive demonstration that the metals in galactic outflows are the source of the metals in the intracluster gas would require the model to include galaxies covering the whole mass range, incorporating the relationship between metal abundance and stellar mass, about which we know quite a lot (§1), and the relationship between outflow rate and stellar mass, about which we as yet know little (Veilleux et al. 2020).

Our estimates of the metal abundance in the SMGs are surprisingly large, often even larger than the values of the metal abundance of the galaxies that are likely to be their descendants. Their descendants in the universe today are likely to be the massive early-type galaxies (§1), which reach a metal abundance of about twice the solar value

(Gallazzi et al. 2005). The immediate descendants of SMGs at $z \sim 4$ seem likely to be the population of quiescent galaxies at $z \sim 3$ (Valentino et al. 2020). There is only one galaxy in this population for which there is a measurement of the metal abundance, which is $\sim 1.8 Z_{\odot}$ (Saracco et al. 2020). In the case of both populations, the values of the metal abundance for the SMGs are often higher than the values for their putative descendants.

Is there a way that the subsequent evolution of the SMG might have reduced its initial metal abundance? The evolutionary route from an SMG, a galaxy with a small physical size but with a huge star-formation rate, to a massive early-type galaxy in the universe today, a galaxy with a large physical size but a low star-formation rate, is still very uncertain (Tacchella et al. 2016). We speculate that it is the sequence of mergers that seems likely to have occurred since the SMG epoch - the obvious way of pumping up the physical size of the galaxy - which might have reduced the initial metal abundance. The ages of the stellar populations of present-day early-type galaxies imply that most of the star formation in one of these galaxies must have happened in the SMG epoch, with relatively few stars (and thus small amounts of metals) having been formed in the subsequent evolution of the galaxy (Thomas et al. 2010). It therefore seems likely that most of the mergers that occurred after the SMG epoch would have been dry mergers, because otherwise there would have been new bursts of star formation. The masses of the SMGs in Table 4 are only a few times lower than the masses of the most massive early-type galaxies today, so it seems likely that most of the mergers would have been minor mergers in which the galaxy that was the direct descendant of the SMG was the largest partner, because otherwise the galaxy would have grown too large by the present day. Given the strong relationship between metal abundance and stellar mass seen at all epochs (§1), it therefore seems likely that each merger would have reduced the metal abundance of the SMG-descended galaxy.

7 CONCLUSIONS

We have measured the mass of metals in 13 submillimetre galaxies (SMGs) at $z \sim 4$ in which the gas, based on previous observations, lies in a cold rotating disk. We measured the metal masses using observations of CO in either the $J = 1 - 0$ or $J = 2 - 1$ lines, observations of atomic carbon in the $C\text{I } 1 - 0$ lines and continuum observations of dust. We used the values of the calibration factors for these tracers obtained by the first attempt to calibrate all three tracers simultaneously (Dunne et al. 2022). For 10 of the 13 galaxies there are observations of at least two tracers and for 7 galaxies there are observations of all three. Our method is independent of the metal abundance in the SMGs, in contrast to the method in which the tracer is used to estimate the total mass of the ISM. We obtained the following results:

- We obtained very similar mass estimates for the different tracers. Our estimates of the mass of metals in the SMGs are similar to the entire metal content of a massive early-type galaxy at the present day.
- There is a well known paradox that when the mass of the ISM in an SMG is estimated from CO observations it is often higher than the dynamical mass. We show that the same is true when the mass of the ISM is estimated from $C\text{I } 1 - 0$ or from dust continuum observations. We argue that the most likely explanation is that the metal abundance in SMGs is higher than in the Galaxy. The alternative explanation is that the ISM in an SMG is different in its chemistry, physics or structure from the ISM in the Galaxy in just such a way that the calibration factors for all three tracers are reduced by a similar factor, which is possible but seems unlikely.

- On the assumption that our explanation of this paradox is the correct one, we used the dynamical masses of the galaxies to set an upper limit on the mass of the ISM in each galaxy, allowing us to set a lower limit on the metal abundance. We found lower limits on Z/Z_{\odot} of between 0.9 and 12.9. The caveat to this result is that we cannot be sure that for most of the galaxies the CO and $C\text{I}$ emission is confined to the region of the dynamical analysis. Our lower limits on the metal abundance are much higher than virtually all the recent measurements of the metal abundance in high-redshift galaxies from JWST observations, although for the one galaxy in our sample for which there is a JWST measurement, the JWST measurement gives a super-solar metal abundance that is consistent with our lower limit.

- We have used chemical evolution models to investigate the cause of the high metal masses and abundances. We show that these are what is expected shortly after the formation of a galaxy if the stellar IMF is top-heavy with a higher fraction of high-mass metal-producing stars than in the Galaxy.

- We use these models to show that the metals in the outflows from these galaxies can explain quantitatively the long-standing conundrum that ≈ 75 per cent of the metals in present-day rich clusters are in the intracluster gas rather than in the galaxies.

- Our estimates of the metal abundance in the SMGs are higher than the values of the metal abundance in the galaxy populations that are their probable descendants. We speculate that the explanation is the gradual dilution of the metal content by a sequence of dry mergers after the SMG epoch.

ACKNOWLEDGEMENTS

We thank Tim Davis for comments on an early version of this manuscript. Stephen Eales and Matthew Smith thank the Science and Technology Facilities Council for support (consolidated grant ST/K000926/1).

DATA AVAILABILITY

The ALMA data referenced in Table 2 is in the ALMA archive. All the other observational data is in published papers.

REFERENCES

- Aravena M., et al., 2016, *MNRAS*, **457**, 4406
 Arellano-Córdova K. Z., et al., 2022, *ApJ*, **940**, L23
 Asplund M., Grevesse N., Sauval A. J., Scott P., 2009, *ARA&A*, **47**, 481
 Bakx T. J. L. C., et al., 2018, *MNRAS*, **473**, 1751
 Barger A. J., Cowie L. L., Sanders D. B., Fulton E., Taniguchi Y., Sato Y., Kawara K., Okuda H., 1998, *Nature*, **394**, 248
 Bolatto A. D., Wolfire M., Leroy A. K., 2013, *ARA&A*, **51**, 207
 Boselli A., et al., 2010, *PASP*, **122**, 261
 Bothwell M. S., et al., 2017, *MNRAS*, **466**, 2825
 Bouché N. F., et al., 2022, *A&A*, **658**, A76
 Cappellari M., et al., 2012, *Nature*, **484**, 485
 Carnall A. C., et al., 2023, *arXiv e-prints*, p. arXiv:2301.11413
 Coppin K. E. K., et al., 2010, *MNRAS*, **407**, L103
 Cullen F., et al., 2019, *MNRAS*, **487**, 2038
 Curti M., et al., 2023, *MNRAS*, **518**, 425
 Daddi E., et al., 2009, *ApJ*, **694**, 1517
 De Vis P., et al., 2017, *MNRAS*, **464**, 4680
 De Vis P., Maddox S. J., Gomez H. L., Jones A. P., Dunne L., 2021, *MNRAS*, **505**, 3228
 Di Teodoro E. M., Fraternali F., 2015, *MNRAS*, **451**, 3021

- Downes D., Solomon P. M., 1998, *ApJ*, **507**, 615
- Dunne L., Maddox S. J., Papadopoulos P. P., Ivison R. J., Gomez H. L., 2022, *MNRAS*, **517**, 962
- Dye S., et al., 2015, *MNRAS*, **452**, 2258
- Dye S., et al., 2022, *MNRAS*, **510**, 3734
- Eales S. A., Wynn-Williams C. G., Duncan W. D., 1989, *ApJ*, **339**, 859
- Eales S., Lilly S., Gear W., Dunne L., Bond J. R., Hammer F., Le Fèvre O., Crampton D., 1999, *ApJ*, **515**, 518
- Eales S., et al., 2012, *ApJ*, **761**, 168
- Eales S., de Vis P., Smith M. W. L., Appah K., Ciesla L., Duffield C., Schofield S., 2017, *MNRAS*, **465**, 3125
- Fraternali F., Karim A., Magnelli B., Gómez-Guijarro C., Jiménez-Andrade E. F., Posses A. C., 2021, *A&A*, **647**, A194
- Gallazzi A., Charlot S., Brinchmann J., White S. D. M., Tremonti C. A., 2005, *MNRAS*, **362**, 41
- Genzel R., et al., 2017, *Nature*, **543**, 397
- Ginolfi M., et al., 2020, *A&A*, **633**, A90
- Harrington K. C., et al., 2021, *ApJ*, **908**, 95
- Heintz K. E., Watson D., 2020, *ApJ*, **889**, L7
- Heintz K. E., et al., 2022, *arXiv e-prints*, p. [arXiv:2212.02890](#)
- Hodge J. A., Carilli C. L., Walter F., de Blok W. J. G., Riechers D., Daddi E., Lentati L., 2012, *ApJ*, **760**, 11
- Hughes D. H., et al., 1998, *Nature*, **394**, 241
- Jiménez-Andrade E. F., et al., 2018, *A&A*, **615**, A25
- Jones G. C., et al., 2017, *ApJ*, **850**, 180
- Jones G. C., Maiolino R., Caselli P., Carniani S., 2019, *A&A*, **632**, L7
- Jones G. C., Maiolino R., Circosta C., Scholtz J., Carniani S., Fudamoto Y., 2023, *MNRAS*, **518**, 691
- Karakas A. I., Lugaro M., Carlos M., Cseh B., Kamath D., García-Hernández D. A., 2018, *MNRAS*, **477**, 421
- Lelli F., Di Teodoro E. M., Fraternali F., Man A. W. S., Zhang Z.-Y., De Breuck C., Davis T. A., Maiolino R., 2021, *Science*, **371**, 713
- Lilly S. J., Eales S. A., Gear W. K. P., Hammer F., Le Fèvre O., Crampton D., Bond J. R., Dunne L., 1999, *ApJ*, **518**, 641
- Lilly S. J., Carollo C. M., Pipino A., Renzini A., Peng Y., 2013, *ApJ*, **772**, 119
- Limongi M., Chieffi A., 2018, *ApJS*, **237**, 13
- Loewenstein M., 2013, *ApJ*, **773**, 52
- Maeder A., 1992, *A&A*, **264**, 105
- Maiolino R., Mannucci F., 2019, *A&ARv*, **27**, 3
- Mernier F., Biffi V., 2022, *arXiv e-prints*, p. [arXiv:2202.07097](#)
- Neeleman M., Prochaska J. X., Kanekar N., Rafelski M., 2020, *Nature*, **581**, 269
- Nomoto K., Kobayashi C., Tominaga N., 2013, *ARA&A*, **51**, 457
- Papadopoulos P. P., Greve T. R., 2004, *ApJ*, **615**, L29
- Papadopoulos P. P., van der Werf P. P., Xilouris E. M., Isaak K. G., Gao Y., Mühle S., 2012, *MNRAS*, **426**, 2601
- Papadopoulos P., Dunne L., Maddox S., 2022, *MNRAS*, **510**, 725
- Peng Y.-j., Maiolino R., 2014, *MNRAS*, **443**, 3643
- Peng B., et al., 2022, *arXiv e-prints*, p. [arXiv:2210.16968](#)
- Planck Collaboration et al., 2016, *A&A*, **594**, A13
- Portinari L., Moretti A., Chiosi C., Sommer-Larsen J., 2004, *ApJ*, **604**, 579
- Renzini A., Andreon S., 2014, *MNRAS*, **444**, 3581
- Reuter C., et al., 2020, *ApJ*, **902**, 78
- Rizzo F., Vegetti S., Powell D., Fraternali F., McKean J. P., Stacey H. R., White S. D. M., 2020, *Nature*, **584**, 201
- Rizzo F., Vegetti S., Fraternali F., Stacey H. R., Powell D., 2021, *MNRAS*, **507**, 3952
- Roman-Duval J., et al., 2022, *ApJ*, **928**, 90
- Romano D., Matteucci F., Zhang Z. Y., Papadopoulos P. P., Ivison R. J., 2017, *MNRAS*, **470**, 401
- Saracco P., et al., 2020, *ApJ*, **905**, 40
- Schaerer D., Marques-Chaves R., Barrufet L., Oesch P., Izotov Y. I., Naidu R., Guseva N. G., Brammer G., 2022, *A&A*, **665**, L4
- Scholtz J., Maiolino R., Jones G. C., Carniani S., 2023, *MNRAS*, **519**, 5246
- Scoville N., et al., 2016, *ApJ*, **820**, 83
- Scoville N., et al., 2017, *ApJ*, **837**, 150
- Smail I., Ivison R. J., Blain A. W., 1997, *ApJ*, **490**, L5
- Spilker J. S., et al., 2016, *ApJ*, **826**, 112
- Spilker J. S., et al., 2018, *Science*, **361**, 1016
- Tacchella S., Dekel A., Carollo C. M., Ceverino D., DeGraf C., Lapiner S., Mandelker N., Primack J. R., 2016, *MNRAS*, **458**, 242
- Tacchella S., et al., 2022, *arXiv e-prints*, p. [arXiv:2208.03281](#)
- Tacconi L. J., et al., 2018, *ApJ*, **853**, 179
- Tacconi L. J., Genzel R., Sternberg A., 2020, *ARA&A*, **58**, 157
- Taylor A. J., Barger A. J., Cowie L. L., 2022, *ApJ*, **939**, L3
- Thomas D., Maraston C., Schawinski K., Sarzi M., Silk J., 2010, *MNRAS*, **404**, 1775
- Valentino F., et al., 2020, *ApJ*, **889**, 93
- Veilleux S., Maiolino R., Bolatto A. D., Aalto S., 2020, *A&ARv*, **28**, 2
- Walter F., Brinks E., Duric N., Klein U., 1997, *AJ*, **113**, 2031
- Yin J., Hou J. L., Prantzos N., Boissier S., Chang R. X., Shen S. Y., Zhang B., 2009, *A&A*, **505**, 497
- Zhang Z.-Y., Romano D., Ivison R. J., Papadopoulos P. P., Matteucci F., 2018, *Nature*, **558**, 260
- da Cunha E., et al., 2013, *ApJ*, **766**, 13
- van den Hoek L. B., Groenewegen M. A. T., 1997, *A&AS*, **123**, 305

APPENDIX A: APPENDIX A: CORRECTION FOR THE EFFECT OF ASYMMETRIC DRIFT

We have made a correction to the dynamical masses for the effect of stellar pressure (asymmetric drift) for the six galaxies for which this correction was not made in the original analysis in the literature, using the formalism given in Appendix A of [Bouché et al. \(2022\)](#). The gravitational potential is given by:

$$\frac{GM(< r)}{r} = v_{\text{rot}}^2 + \eta \sigma^2 \left(\frac{r}{r_d} \right) \quad (\text{A1})$$

in which v_{rot} is the rotational velocity, σ is the velocity dispersion, r_d is the scale length of the disk, and η is a numerical constant of order unity. The value of η depends on the model assumed for the disk ([Bouché et al. 2022](#)). We have assumed a value of 1 appropriate for a disk in which the disk thickness and velocity dispersion have no radial dependence. The fractional correction to the masses for asymmetric drift is given by the ratio of the second to the first term on the righthand side of the equation. We have estimated this from the data in the original papers, and our estimates are listed in Table 4. For all but two galaxies the correction is ≤ 10 per cent. We have used these estimates to correct the masses for asymmetric drift for the seven galaxies in the sample for which this effect was not included in the original analysis.

This paper has been typeset from a \LaTeX file prepared by the author.